PROCEEDINGS A

rspa.royalsocietypublishing.org

Research

Cite this article: Milne IA, Sharma RN, Flay RGJ. 2017 The structure of turbulence in a rapid tidal flow. *Proc. R. Soc. A* **473**: 20170295. http://dx.doi.org/10.1098/rspa.2017.0295

Received: 21 April 2017
Accepted: 26 July 2017

Subject Areas:
ocean engineering, oceanography

Keywords:
turbulence, tidal energy, boundary layer flow

Author for correspondence:
I. A. Milne
e-mail: ian.milne@uwa.edu.au

Electronic supplementary material is available online at https://dx.doi.org/10.6084/m9.figshare.c.3849784.

THE ROYAL SOCIETY PUBLISHING

The structure of turbulence in a rapid tidal flow

I. A. Milne[1], R. N. Sharma[2] and R. G. J. Flay[2]

[1]Centre for Offshore Foundation Systems, The University of Western Australia, Crawley 6009, Australia
[2]Department of Mechanical Engineering, The University of Auckland, Auckland 1010, New Zealand

IAM, 0000-0002-8552-2208

The structure of turbulence in a rapid tidal flow is characterized through new observations of fundamental statistical properties at a site in the UK which has a simple geometry and sedate surface wave action. The mean flow at the Sound of Islay exceeded 2.5 m s^{-1} and the turbulent boundary layer occupied the majority of the water column, with an approximately logarithmic mean velocity profile identifiable close to the seabed. The anisotropic ratios, spectral scales and higher-order statistics of the turbulence generally agree well with values reported for two-dimensional open channels in the laboratory and other tidal channels, therefore providing further support for the application of universal models. The results of the study can assist in developing numerical models of turbulence in rapid tidal flows such as those proposed for tidal energy generation.

1. Introduction

In comparison with the atmospheric boundary layer, there remains a lack of measurements of turbulence properties reported for highly energetic tidal flows (i.e. Reynolds numbers $Re = UD/\nu$ $\mathcal{O}(1 \times 10^8)$, where U is the mean velocity, D is the channel depth and ν is the kinematic viscosity) such as those targeted for tidal energy generation [1]. Properties which inform the turbulence structure and scales such as the anisotropic ratios, Reynolds stresses, total turbulent kinematic energy and spectra are important to quantify due to their use in turbulence closure models and for assessing the turbulent loading of tidal energy generation systems [2].

For well-mixed tidal flows, the turbulence has previously been considered to be analogous to that of an open-channel flow [3]. Extensive bodies of research into steady two-dimensional open-channel flows in the laboratory have led to the development of universal laws and promoted simple turbulence closure models [4]. A region of approximately constant stress is considered to exist near the bed in which the velocity profile exhibits a logarithmic dependency on elevation and where production exceeds the rate of dissipation. Further from the bed, the production and dissipation are approximately in equilibrium. The Reynolds stresses also exhibit an inversely proportional relationship with elevation. The anisotropic ratios and the correlation coefficients which inform the turbulence structure have been found to tend towards near-constant values in the equilibrium region of the water column and to be only weakly dependent on the Reynolds number. These laboratory studies have also demonstrated the highly intermittent nature of the Reynolds stresses. This behaviour is considered to be associated with a well-defined sequence of events dominated by sweeping and ejection motions of horseshoe-like coherent structures near the seabed. Demonstrating that these laws and characteristics are applicable to fast-flowing tidal channels in nature could greatly facilitate the development of numerical models of turbulence for such flows.

Early observations of turbulence in tidal channels were presented in [5–9] for instance, which typically employed electro-current meters. These works provided support for universal laws based on surface similarity theory and the hypothesis of Kolmogorov [10] to describe the distributions of the turbulence scales and the intermittent nature of the Reynolds stress, which is associated with the presence of coherent turbulent structures. Support has also been found for the application of empirical models which were originally developed for atmospheric boundary layers to describe the turbulent spectra of a marine boundary layer [11,12]. The vast majority of these preceding cited studies are, however, based on measurements close to the bed or in relatively slow flows as sediment transport has been the primary underlying focus.

Measurements of turbulence at greater elevations and in more rapid flows such as those suited to the exploitation of tidal energy are inherently technically challenging to obtain. Advances in sensor technology and the introduction of acoustic-Doppler current profilers (ADCPs) and velocimeters (ADVs) in particular have, however, enabled the turbulence intensities, stresses and spectra to be measured unobtrusively at tidal energy sites such as at the Fall of Warness, UK [13,14], and Puget Sound, USA [15,16], and can therefore assist in quantifying the turbulence structure and dominant scales above the seabed. Deployments which use a set-up comprising a bottom-mounted ADCP and ADV, such as that employed for the Puget Sound study [15], are particularly attractive in that they can minimize potential errors due to sensor motion and offer independent estimates of the Reynolds stresses, and the ADV can be used to measure the anisotropy, which cannot be reliably obtained using a standard four-beam ADCP.

In this study, fundamental statistical properties obtained from new observations at the Sound of Islay, UK, are presented and, together with results from the limited reported studies at other tidal energy sites, are used to investigate the applicability of universal scaling laws and empirically derived correlations of turbulence in open-channel flows to describe the turbulence in strong tidal flows. The new data are particularly novel in that the Sound of Islay is subject to tidal currents with mean velocities exceeding $2.5\,\mathrm{m\,s^{-1}}$, it has a well-mixed flow and, in contrast with other studied sites, it has a relatively simple geometry with minimal secondary flows. Furthermore, the surface waves are relatively sedate with significant wave heights generally less than 1 m and peak wave periods ranging between 6 and 10 s. As such, the hydrodynamic conditions are considered to be particularly well suited to drawing comparisons with canonical two-dimensional open-channel flows and therefore to validating empirical models proposed for such flows. This study extends the work of Milne *et al.* [17] by including distributions of the mean flow and turbulent properties through the water column and specifically characterizing the Reynolds stresses, wavenumber spectra and higher-order statistics.

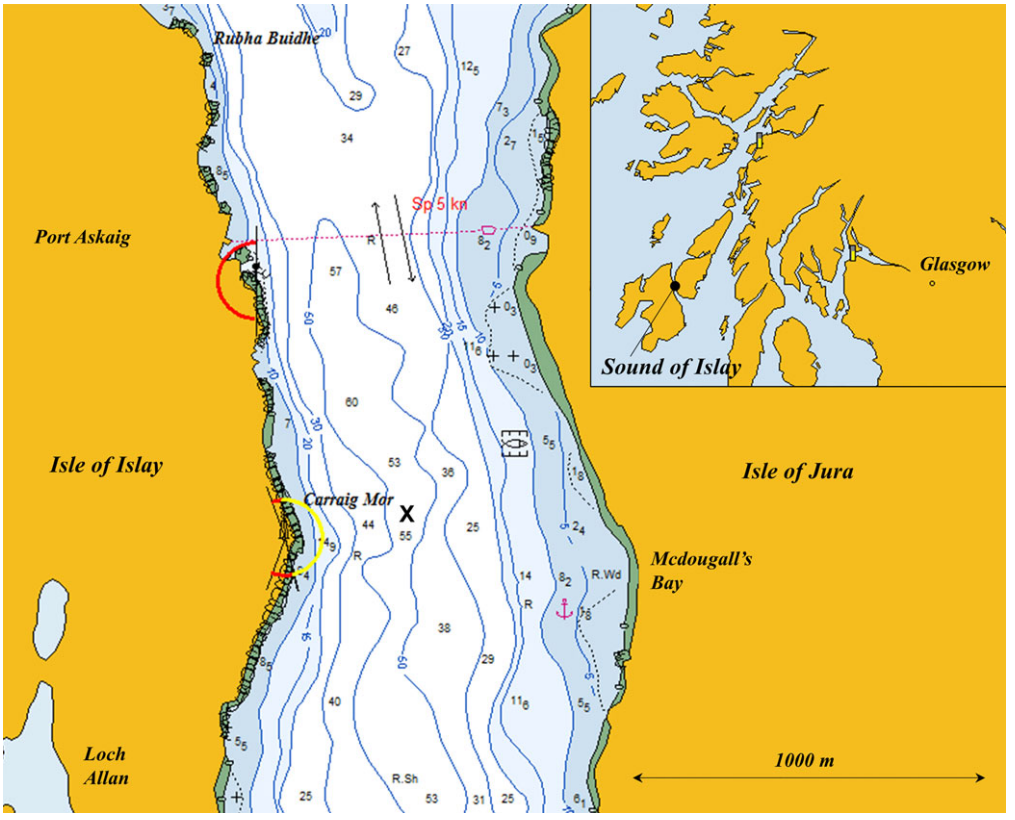

Figure 1. Map of the Sound of Islay, aligned north, with depth contours (metres) and the data acquisition site indicated by 'X'. The location of the Sound of Islay in the Inner Hebrides of Scotland, UK, is shown top right. (Adapted from Admiralty Charts acquired from the UK Hydrographic Office (http://www.ukho.gov.uk).) (Online version in colour.)

2. Material and methods

(a) Study site

The observations were made in the central section of the Sound of Islay, which is a tidal channel approximately 30 km in length flowing nearly north to south between the Isles of Islay and Jura in the Inner Hebrides of Scotland, UK. The measurements were obtained at the grid reference N 55 50.432′, W 006 05.900′ where the width is approximately 800 m and the depth 55 m as shown in figure 1. The measurement site corresponds approximately with the location of a proposed tidal turbine array. The flow is well mixed and the site is characterized by a seabed that descends steeply from the shore and comprises boulders, rock and gravel, with little fine sediment. The landmasses of both islands protect the site from significant wind-induced wave action.

(b) Analysis techniques

The data were acquired using a set-up comprising both an ADCP and an ADV which were positioned within close proximity on a steel frame that was deployed on the seabed, as shown in figure 2. As detailed by Milne [1], the TRDI 1.2 Mhz Workhorse ADCP was configured to continuously record the velocities in a direction aligned with the beams of the sensors. The four diverging beams were inclined at an angle of $\theta = 20^\circ$ from the vertical and were arranged in a Janus configuration (i.e. at 90° azimuths about the vertical (z)-axis). The measurements were acquired at a sampling frequency of 2 Hz and at 1 m vertical intervals to the surface, with the lowest recording at an elevation of $z = 4$ m above the seabed.

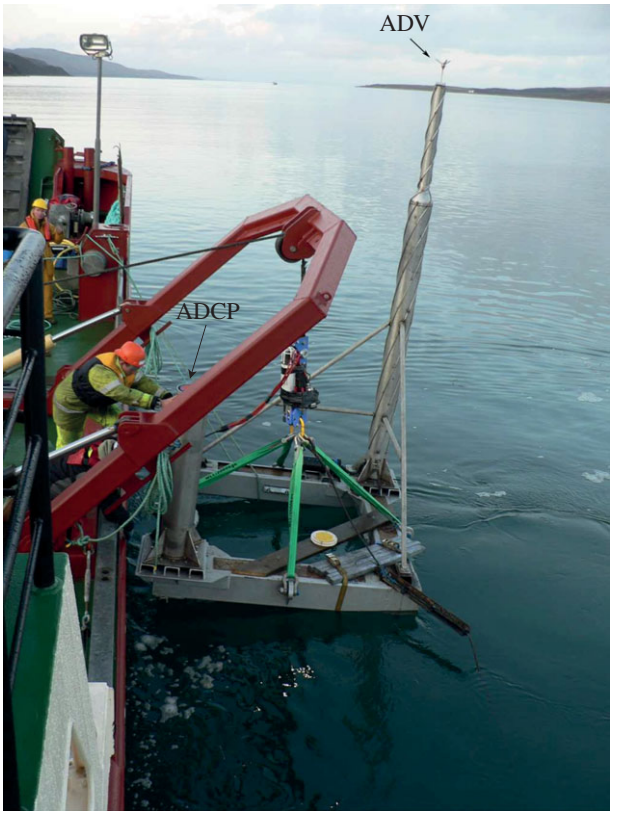

Figure 2. The rig prior to deployment on the seabed showing the ADCP and ADV arrangement. (Photo supplied courtesy of Partrac Ltd (http://www.partrac.com).) (Online version in colour.)

The ACDP data were used to inform the distributions of the mean velocities and turbulent properties such as the Reynolds stresses, turbulent production and dissipation, and the mixing length. The Reynolds stresses (considered hereafter in terms of the velocity covariances) were estimated from the ADCP measurements by employing the variance technique [18], in which

$$-\sigma_{uw} = \frac{\sigma_{b2}^2 - \sigma_{b1}^2}{2\cos 2\theta}, \tag{2.1}$$

where $\sigma_{b_i}^2$ is the variance of the fluctuating velocity measured along the direction of the ith beam. This approach inherently assumes that the second-order moments are statistically homogeneous across the lateral separation of the beams and the sensor tilt is small. For the present study, the relatively small (i.e. less than 5°) tilt angles of the sensor were considered to result in an error of approximately 10% in the stresses [1]. The comparisons between the independent ADV and ADCP estimates of the Reynolds stress, which are shown later, demonstrate that this error does not significantly affect the results or the conclusions of the study. Furthermore, given that the mixing length is proportional to σ_{uw}^2, the error in these estimates was considered to be only approximately 5%.

The rate of turbulence dissipation, ε, was estimated from the ADCP beam velocity measurements using the structure function method. The approach entails calculating the mean square of the velocity fluctuation difference between two points separated by a distance r through the expression [19]

$$D(z,r) = \overline{(b_i(z) - b_i(z+r))^2}. \tag{2.2}$$

A regression technique was used to estimate the dissipation from the turbulent cascade model given as $D(z,r) = C_v^2 \varepsilon^{2/3} r^{2/3}$, where the value of the constant $C_v = 2.0$.

A Nortek Vector ADV was used to measure all three fluctuating velocities at a fixed point at an elevation of 5 m above the seabed. The ADV was mounted in an upright configuration at the top of a steel mast which was affixed to the base frame. The ADV sampled the velocities at a frequency of 4 Hz continuously over the duration of the experiment. The vector measurements were acquired in the beamwise coordinate system aligned with the transducers of the sensors and were then transformed to obtain the Cartesian velocities u (streamwise), v (transverse) and w (vertical). This transformation process corrected for sensor tilt and aligned the streamwise velocities with the mean velocity direction for each sample. The velocities measured by the ADV were subsequently used to directly quantify the standard deviations of velocity, the Reynolds stress, total turbulent kinetic energy, spectra and the higher-order statistical moments above the seabed. Further details on the processing of the ADCP and ADV measurements as well as the quality control measures that were employed are provided by Milne [1].

3. Results

(a) Mean velocity and turbulence through the water column

Here, we focus on observations during the spring tide in November 2009, in which mean tidal velocities exceeding $2.5\,\mathrm{m\,s^{-1}}$ were observed at the Sound of Islay. These data were a subset of a larger 29 day acquisition period. As reported by Milne [1], during the spring tide the directionality of the flow was near uniform through the water column and the surface waves were small with heights generally less than 1 m. The water level variation was also relatively small at approximately 1 m. The strong currents arise due to the difference in the tidal phase around the islands and are influenced to a comparatively small degree by the tidal range.

The evolution of the boundary layer over the spring tide is demonstrated through the hourly mean velocity profiles shown in figure 3. The boundary layer developed rapidly from slack flow and the thickness (considered to correspond to the elevation where $U = 99\%$ of the maximum velocity) was at least 50 m during the peak flood flow and was a maximum of approximately 40 m during the ebb. The profiles have also been plotted with a logarithmic ordinate, which demonstrates that the mean velocity variation took an approximately logarithmic form for elevations up to approximately 10 m above the seabed (i.e. $z/h \lesssim 0.2$). Estimates of the friction velocity from fitting the profiles to a law of the wall model were, however, not able to be computed with sufficient confidence due to the limited data points and measurements not extending to lower elevations.

In general, there were no indications in the profiles that strong secondary subsurface currents were present. The profiles reveal asymmetries between the acceleration and deceleration of the flood and ebb tides. In particular, the boundary layer thickness was greater during periods of deceleration than during acceleration of the tidal flow, which suggests that, once generated, the large eddies persisted after the maximum flow. However, at maximum ebb flow (profile 10) the thickness appears to have reduced considerably to approximately 25 m, implying that the boundary layer thickness was, however, relatively dynamic over the tidal cycle.

Profiles of the Reynolds stresses corresponding to the equivalent periods of the tidal cycle as the mean velocity profiles are also shown in figure 3. The largest stresses were observed near the bed and at around peak tidal flow. The stresses tended to very small values near the top of the water column for the peak flood. For ebb flow, the stresses were approximately zero at around $z = 40$ m, with the exception of profile 10, where they tended towards zero at $z = 25$ m. Together, these results are consistent with the thickness of the boundary layer observed during the tidal cycle. During the ebb, the variation in the stress was approximately inversely proportional to the elevation. This relationship was somewhat poorer for the flood profiles, where regions approximately 10 m in height were observed where the stresses deviated significantly from the inversely proportional form.

The variations in the mean shear $S = \mathrm{d}U/\mathrm{d}z$, turbulent energy shear production $P = -\sigma_{uw}S$, rate of dissipation ε and the mixing length $l_\mathrm{m} = (-\sigma_{uw})^{1/2}/S$ corresponding to profiles 5 and

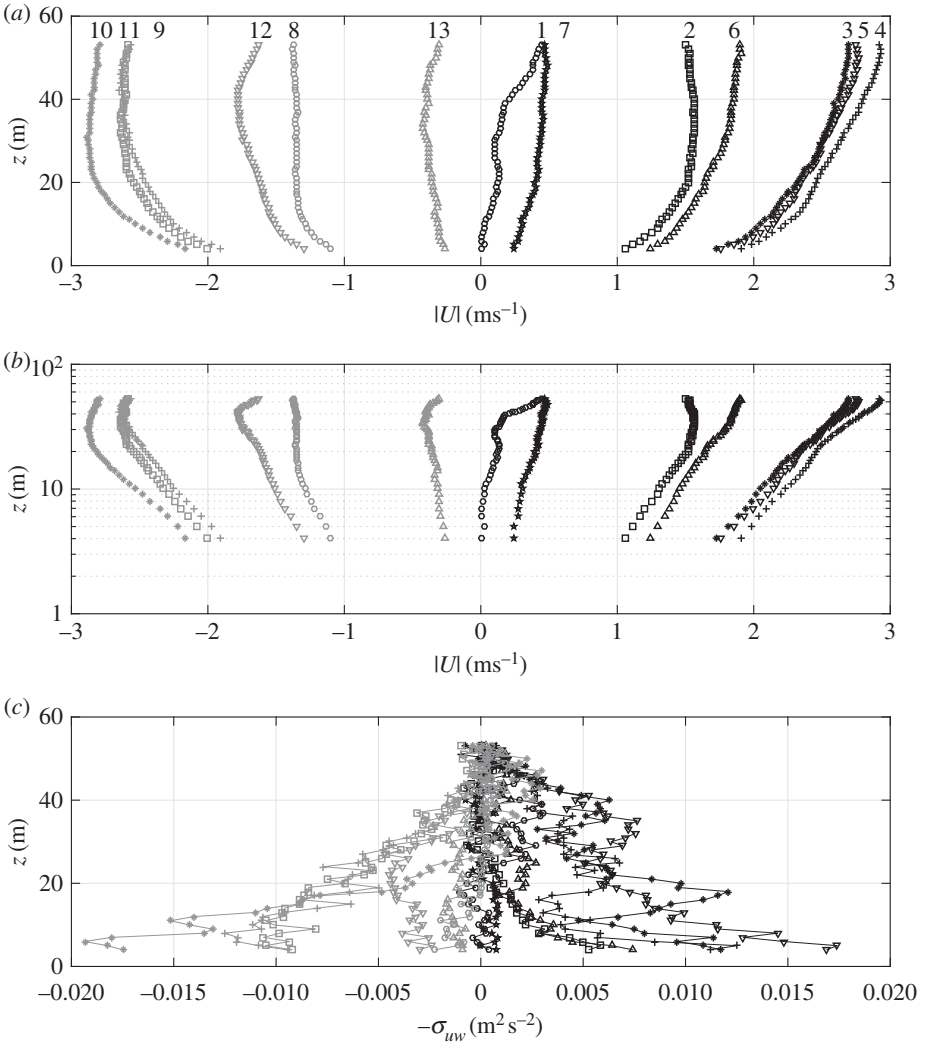

Figure 3. Vertical profiles of the mean streamwise velocity (*a*,*b*) and Reynolds shear stress (*c*) at consecutive hourly intervals during the tidal cycle (the first profile corresponds to the beginning of the flood tide).

11, which are representative of the observations around peak flow, are presented in figure 4. The approximately linear variation in the shear in the region near to the bed ($z \leq 10$ m) further elucidates the law of the wall-like behaviour. In this region, the shear took near-equivalent values during the flood and ebb. Further from the bed, the shear decreased approximately linearly during the ebb, but the variation was less linear during the flood. The turbulent energy production was greatest close to the seabed and decayed rapidly with increasing elevation. Its magnitude was similar to the rate of dissipation for elevations between 15 and 30 m above the seabed, while closer to the bed the production exceeded the dissipation. The profiles for the ebb show that the dissipation exceeded the production at elevations above 30 m, which is also in qualitative agreement with the characteristics of the free-surface region in an open-channel flow. It can be noted that for the flood, however, the production exceeded the dissipation at approximately $z = 35$ m. This corresponds to the elevation at which the shear increased in magnitude and thus differed from the open-channel flow behaviour. The profiles show that, near the bed, the mixing length varied approximately linearly with the increase in elevation, with similar values for the flood and ebb tides. Further from the bed, asymmetries were observed between the flood and

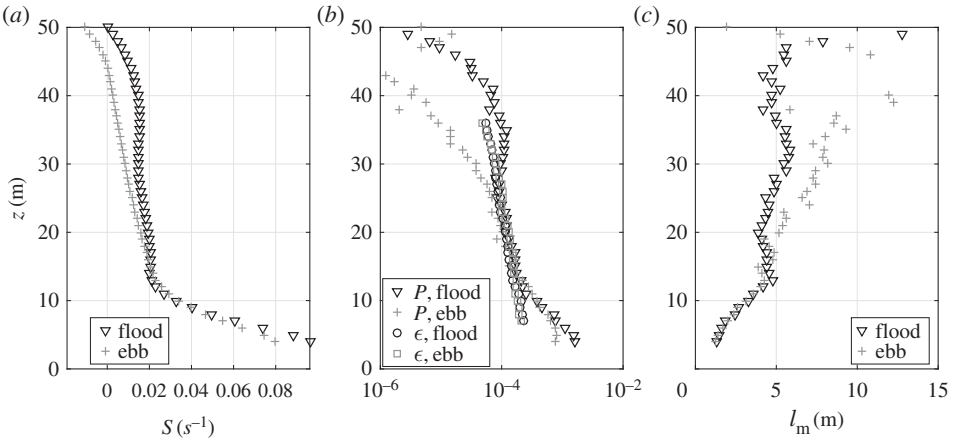

Figure 4. Vertical profiles of the mean shear (*a*), turbulent energy production and dissipation (*b*), and the mixing length (*c*) at peak flood and ebb tidal flow (corresponding to profiles 5 and 11 in figure 3).

ebb profiles. During the flood, the mixing length profile flattened and tended to a value of approximately 5 m. By contrast, for the ebb the mixing length continued to increase approximately linearly with elevation and had a value of approximately 10 m near the top of the water column.

(b) Turbulence structure above the seabed

Figure 5 shows the time histories of the 5 min mean velocity and the corresponding records of the Reynolds stress, the standard deviations of the fluctuating velocities and the total turbulent kinetic energy ($q^2 = 0.5(\sigma_u^2 + \sigma_v^2 + \sigma_w^2)$) at an elevation of 5 m above the seabed during the flood–ebb tidal cycle. Estimates of the mean velocity and Reynolds stress from both the ADV and ADCP are presented for comparison. The magnitudes of all these statistics varied approximately in phase with the mean tidal flow and exhibited short-term fluctuations of less than 15 min. These events generally corresponded to variations in the mean velocity and were likely to be associated with the unsteady nature of the mean tidal velocity and the boundary layer, as opposed to turbulent structures. The anisotropic ratios derived from these results are also shown in figure 5 and serve to elucidate the turbulence structure. These ratios tended to near-constant values of $\sigma_v/\sigma_u = 0.75$ and $\sigma_w/\sigma_u = 0.55$ during non-slack periods of the tidal flow. We have also plotted the ratio $-\sigma_{uw}/q^2$ and the correlation coefficient $-\sigma_{uw}/\sigma_u\sigma_w$. These latter ratios also tended to approximately constant values, implying that the Reynolds stress and the intensities were closely related.

Velocity spectra and co-spectra at an elevation of 5 m are shown in figure 6 as a function of the non-dimensional wavenumber $k^* = 2\pi fz/U$ (where f is the frequency in Hz) in order to facilitate testing of the similarity scaling law. These spectra were obtained from 30 samples around peak flood flow of a single tidal cycle which were each linearly detrended and normalized by the variance and then averaged and smoothed at high wavenumbers for clarity. Similar results were also found for peak ebb flow conditions. The spectra show that the streamwise energy encompassed a relatively broad range of spectral scales, with a peak centred approximately $k^* \approx 0.4$ during both the flood and ebb. By contrast, the spectral energy band of the lateral and vertical motion was comparatively more restricted with peaks corresponding to higher wavenumbers of approximately $k^* = 2$ and 4, respectively. At higher wavenumbers, the velocity spectra appear to tend towards a $k^{*-2/3}$ proportionality, while the co-spectra tend towards $k^{*-4/3}$, both of which are suggestive of isotropic-like behaviour. For the streamwise spectra, this proportionality occurs at $k^* > 2$, while the vertical motion appears to correspond to higher wavenumbers of approximately $k^* > 8$.

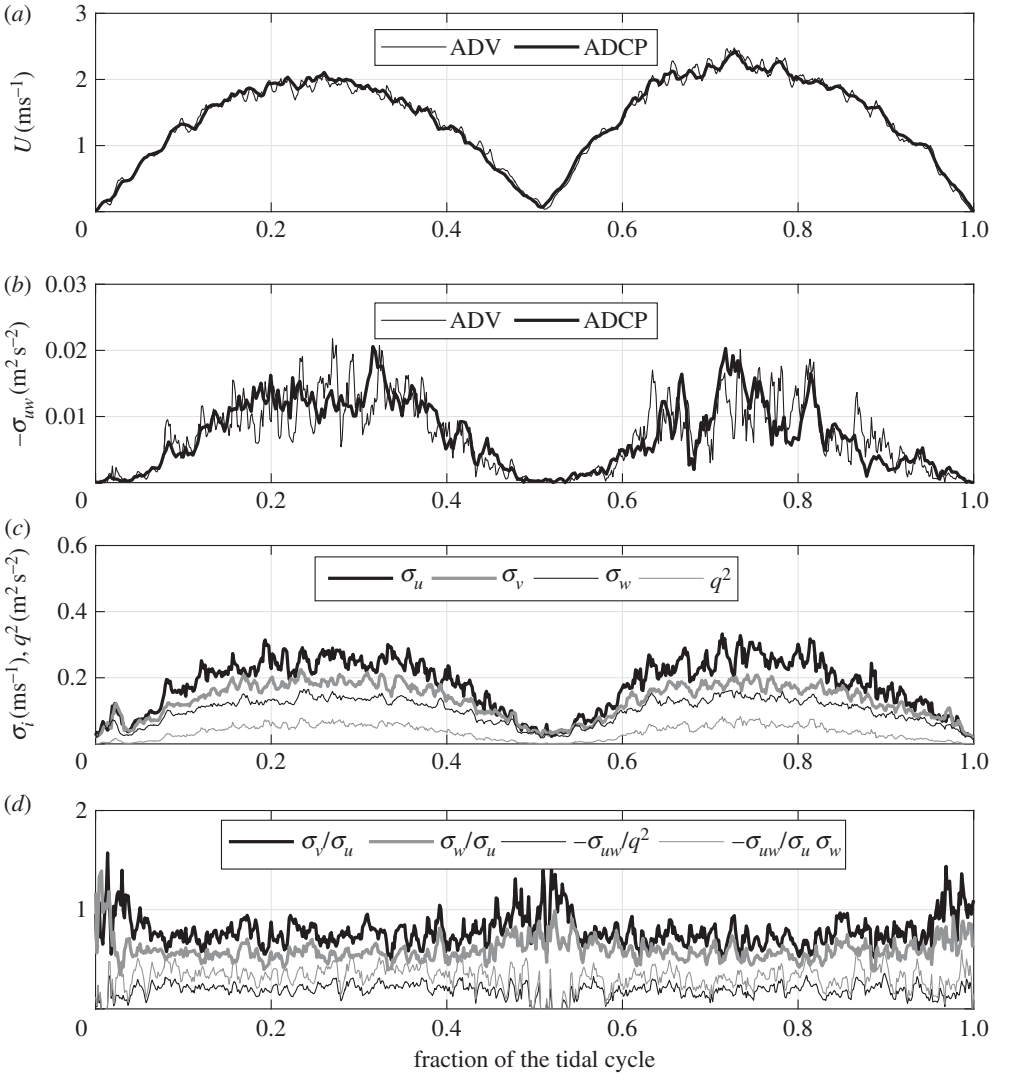

Figure 5. Time histories of the (*a*) mean streamwise velocity; (*b*) Reynolds stress; (*c*) standard deviations of the velocity fluctuations and the total turbulent kinetic energy; and (*d*) the ratios of the second-order turbulence statistics at an elevation of 5 m above the seabed observed during the spring (flood then ebb) tidal cycle. (*c*,*d*) Comprising ADV measurements only.

The higher-order statistical moments, the skewness (S_{ij}) and kurtosis (K_{ij}) provide additional insights into the underlying nature of the Reynolds stress. Time histories of these statistics for the Reynolds stress over the flood–ebb tidal cycle are presented in figure 7 and are compared with the results for the streamwise and vertical velocities. The histories indicate that, while the behaviour of u and w was approximately normal, the Reynolds stresses were skewed and highly kurtosed. We have also presented the intermittency factor γ, which may be used to identify departures from normal behaviour. The intermittency factor has previously been used as an indicator of the proportion of the time in a total record length for which the Reynolds stress is effectively switched on [7]. The factor is related to the kurtosis by $K_{uw} = 3/\gamma$ and its value is shown to have generally varied between 0.25 and 0.33 at Islay.

The contributions from various events to the instantaneous Reynolds stress were investigated using conditional-sampling quadrant theory. The theory has been applied extensively in the literature to study coherent structures in boundary layers. Following Lu & Willmarth [20], the

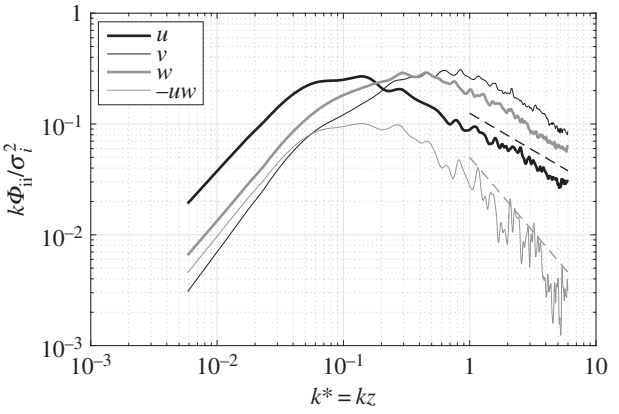

Figure 6. Normalized wavenumber velocity spectra at an elevation of 5 m at peak flood tidal flow. The dashed lines denote the $k^{*-2/3}$ and $k^{*-4/3}$ proportionally.

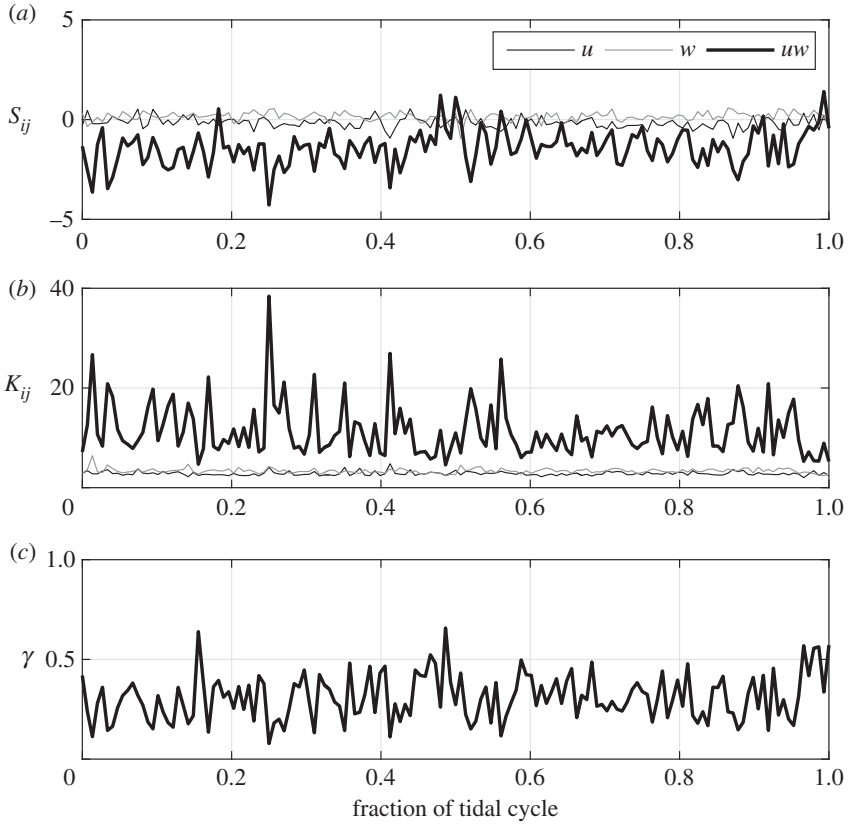

Figure 7. Time histories of the skewness (*a*), kurtosis (*b*) and intermittency (*c*) of the fluctuating velocities *u*, *w* and *uw* at an elevation of 5 m above the seabed.

$u - w$ plane was divided into four quadrants and a 'hole' region. Each quadrant is considered to represent an event related to the bursting phenomenon of horseshoe-like vortices: sweep-like ($u > 0$, $w < 0$), ejection-like ($u < 0$, $w > 0$), inward interaction ($u < 0$, $w < 0$) and outward interaction ($u > 0, w > 0$). The 'hole' is bounded by the curves corresponding to constant Reynolds

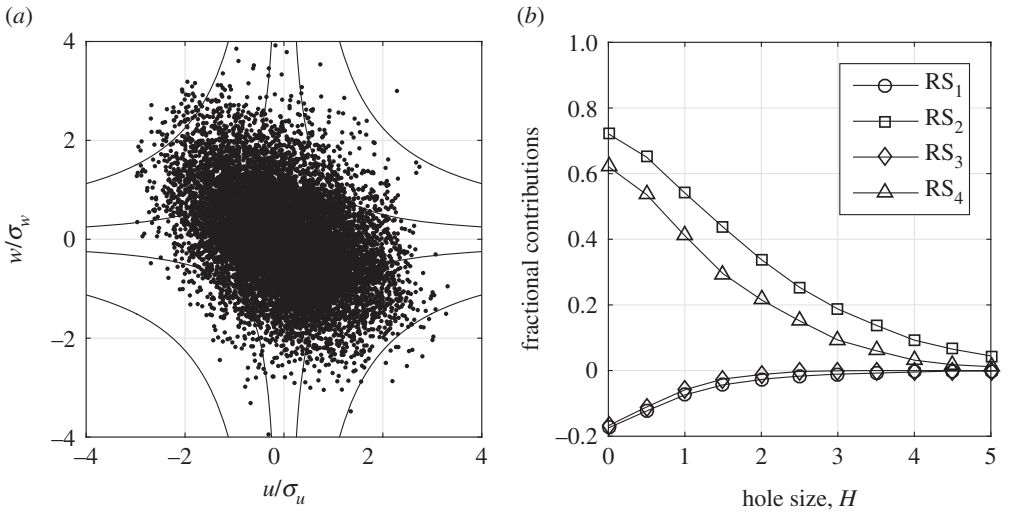

Figure 8. (*a*) Quadrant diagram of the normalized instantaneous fluctuating velocities u and w. The solid lines denote hole sizes of $H = 1$ and $H = 4.5$. (*b*) Fractional contributions to the fluctuating velocities as a function of hole size.

stress. The results shown in figure 8 were obtained at peak tidal flows and show that the stresses were dominated by sweeps and ejections, which is consistent with the literature. Figure 8 also shows the fractional contributions to the Reynolds stress as a function of the hole size, i.e.

$$\mathrm{RS}_i(H) = \int_H^\infty v p_i(v)\,\mathrm{d}v \geq 0, (i = 2, 4) \quad \text{and} \quad \mathrm{RS}_i(H) = \int_{-\infty}^{-H} v p_i(v)\,\mathrm{d}v \leq 0, \quad (i = 1, 3), \tag{3.1}$$

where $v(t) = u(t)w(t)/\sigma_{uw}$ is the normalized instantaneous Reynolds stress fluctuation and $p_i(v)$ is the probability density function. These results demonstrate that, with $H = 0$, the ejection-like events have the largest contribution, constituting approximately 80% of the local Reynolds stress. The sweep-like events have the second largest contribution, of approximately 55%. The contributions from the interaction events RS_1 and RS_3 are negative and are relatively small. The sweep-like events decrease rapidly with the increase in hole size. Only the ejection-like events contribute to the Reynolds stress for hole sizes of $H = 4$ and larger.

4. Discussion

The new measurements at the Sound of Islay provide a valuable addition to the limited reported data for rapid tidal flows and a new opportunity to examine the applicability of empirical models of turbulence. The observation that the boundary layer at the Sound of Islay occupied the majority of the water column is consistent with reports from other tidal flows such as the Cordova Channel, Canada [21]. Together with a logarithmic distribution in the mean velocity at elevations of $z/h < 0.2$ and the approximately inversely proportional relationship observed between the Reynolds stress and elevation, it suggests that the turbulence was primarily mechanical and consistent with a two-dimensional open-channel flow [4]. However, while this aligns with findings at other sites such as Three Mile Slough, USA [3], it is important to note that they are likely to be somewhat reflective of the topography and simple nature of the site and may not be applicable to all rapid tidal flows. The Reynolds stress profiles reported by Osalusi *et al*. [13] at the Fall of Warness, which is more exposed to strong winds for instance, were less linear, particularly in the upper water column.

As estimates of the diffusion of pressure and turbulent energy were not able to be obtained from the experimental set-up, the complete dynamical balance was unable to be tested. However, if these terms are assumed to be relatively small, then the finding that the production was of the same order of magnitude as the dissipation does qualitatively support the notion of an

equilibrium layer at elevations above $z/h \approx 0.2$ and a production-dominated region closer to the bed consistent with that expected for an open-channel flow [4]. The mixing length estimates are also in reasonably good agreement with values for two-dimensional open channels where they have been found to tend to a value of $l_m \approx 0.13D = 7.5$ m in the upper water column (i.e. $z/D \gtrsim 0.6$) [4]. However, the observed values of the mixing length scale underestimate those predicted for a constant stress region (i.e. where $l_m \approx \kappa z$) by approximately 25%. This comparison is particularly useful as it demonstrates the applicability of this length scale as a method of turbulence closure for rapid tidal flows in channels of simple geometry.

The measurements of the anisotropic ratios provide a quantification of the turbulence structure at an elevation of z/h. The observed values agree favourably with the two-dimensional steady flow laboratory results of $\sigma_v/\sigma_u = 0.71$, $\sigma_w/\sigma_u = 0.55$, $-\sigma_{uw}/q^2 = 0.10$ and $-\sigma_{uw}/\sigma_u\sigma_w = 0.40$ [4]. This supports the notion that the ratios are not significantly dependent on the Reynolds number, which was postulated by Nezu & Nakagawa [4]. Comparisons with the atmospheric observations of $\sigma_v/\sigma_u = 0.80$ and $\sigma_w/\sigma_u = 0.68$ reported by Busch [22] suggest that the anisotropy is more pronounced in a tidal channel than in the atmospheric boundary layer. The close relationship identified between the turbulent kinetic energy and the Reynolds stress provides further support for the use of the ratio $-\sigma_{uw}/q^2$ as a simple turbulence closure model, as proposed by Bradshaw *et al.* [23] under well-mixed conditions. The observed value of the ratio is consistent with the result $-\sigma_{uw}/q^2 = 0.14$, which was reported at an elevation of $z/h = 0.06$ during peak flow at the Puget Sound [24]. It is slightly smaller than the value of 0.15 assumed by Bradshaw *et al.* [23], but the latter is deemed to be more applicable to greater elevations from the bed and within the intermediate flow region.

The finding that the spectral peak of the streamwise velocity corresponds to a length scale similar to the depth of the channel is consistent with the observations in the Puget Sound [15] and implies that the most energetic scales were not governed directly by the presence of the boundary but rather the channel depth. Furthermore, the finding that the dominant vertical eddies have a length scale around z is in line with the work of Townsend [25] and the notion that their size is significantly constrained by the seabed. The observation of a co-spectral peak at $k^* = 1$ also implies there were significant contributions to the flux from wavelengths greater than the distance to the bed, which may be due to flattened out eddies [9]. The inception of an integral subrange in the vertical motion at non-dimensional wavenumbers of approximately $k^* = 6$ is similar to that reported at the sites investigated in [7,8,26] ($k^* > 5$) and [11]. Together, the observations at Islay therefore provide further support for the dominant vertical motion and momentum flux energy near the bed of a marine boundary layer being able to be described by the similarity law.

It is also of interest to examine the validity of model spectra which have been previously used to numerically simulate marine turbulence and have been tested for slower tidal flows. Figure 9 shows a comparison of the observed spectra from the ADV point measurements and the von Kármán [27] and Kaimal [28] spectral forms at an elevation of $z = 5$ m above the seabed. The von Kármán spectra were developed on the assumption that the turbulence is homogeneous and isotropic, with the streamwise and vertical spectra expressed, respectively, as

$$\Phi_{uu} = \sigma_u^2 \frac{2L_u}{\pi} \frac{1}{(1 + (1.339L_u k)^2)^{5/6}} \tag{4.1}$$

and

$$\Phi_{ww} = \sigma_w^2 \frac{2L_w}{\pi} \frac{1 + (8/3)(2.678L_w k)^2}{(1 + (2.678L_w k)^2)^{11/6}}. \tag{4.2}$$

With the use of the values of the streamwise and vertical integral length scales of $L_x = 11$ m and $L_w = 2$ m reported by Milne [1] at $z = 5$ m, the model provides a reasonable description of the streamwise spectra but the agreement in the vertical velocity spectra is poorer with the dominant vertical spectra having been shifted towards lower wavenumbers. The empirical Kaimal model was devised using Monin–Obukhov similarity theory and measurements within an atmospheric turbulent boundary layer over flat, uniform terrain. For neutral stability conditions

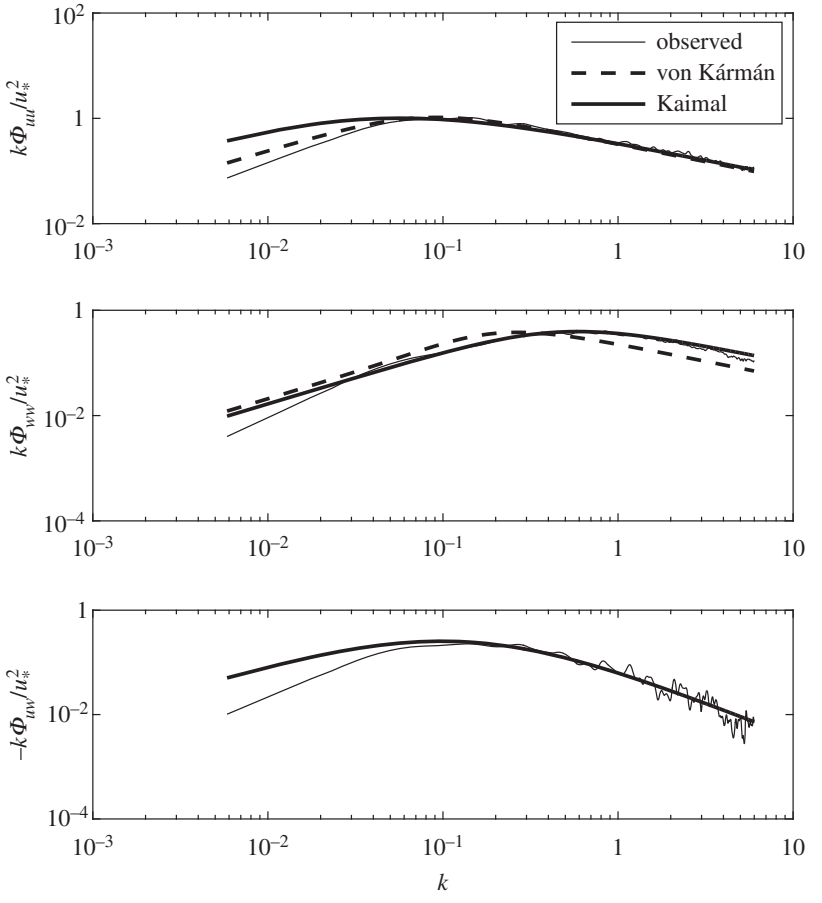

Figure 9. Comparison of the observed spectra with the von Kármán and Kaimal model distributions at an elevation of $z = 5$ m above the seabed.

the streamwise, vertical velocity and co-spectra are given as

$$\Phi_{uu} = \frac{105}{2\pi} u_*^2 z \left(1 + 33\frac{kz}{2\pi}\right)^{-5/3}, \tag{4.3}$$

$$\Phi_{ww} = \frac{2}{2\pi} u_*^2 z \left[1 + 5.3\left(\frac{kz}{2\pi}\right)^{5/3}\right]^{-1} \tag{4.4}$$

and

$$\Phi_{uw} = -\frac{14}{2\pi} u_*^2 z \left(1 + \frac{9.6}{2\pi} kz\right)^{-7/3}, \tag{4.5}$$

where the values of u_*^2 were assumed to be equal to the Reynolds stress obtained directly from the ADV measurements. The Kaimal model overpredicts the energy content at the lowest wavenumbers of the streamwise and co-spectra, but the agreement is much more favourable for the vertical velocity spectrum. These findings are consistent with the studies by Lien & Sanford [11] and Walter *et al.* [12] and reinforces the notion that the vertical eddies are much more affected by the presence of the seabed and that the similarity scaling is appropriate for their description.

Finally, the observed values of the skewness and kurtosis of the Reynolds stresses have been compared with theoretical values which were presented as a function of the correlation coefficient $\sigma_{uw}/\sigma_u\sigma_w$ [29]. For values of the correlation coefficient of between 0 and −1, the skewness is predicted to vary between 0 and −2.82 and the kurtosis between 9 and 15. These results are therefore in close agreement with the observations at Islay. The intermittency factor values of

between 0.25 and 0.33 observed at Islay are also in good agreement with those reported for the Irish Sea and Menai Strait, UK [7], as well as those measured in the laboratory [4]. The results of the quadrant analyses are particularly interesting in that they coincide well with the values derived by Nezu & Nakagawa [4] for the ejection and sweep contributions of $RS_2 = 0.77 \pm 0.029$, $RS_4 = 0.57 \pm 0.029$, which were based on equilibrium conditions. The finding that only ejection-like events contribute for $H = 4.5$ and larger is also consistent with that of Lu & Willmarth [20]. Together, these results provide further support for the notion that the turbulence characteristics in rapid tidal flows may be informed from both laboratory results and observations in tidal channels.

5. Conclusion

The observations presented within this study have provided an opportunity to draw further insights into the fundamental characteristics of the turbulence in a rapid tidal flow. The vertical profiles of the mean flow and turbulence at the Sound of Islay were found to exhibit characteristics that were qualitatively consistent with the form expected for a two-dimensional open-channel flow. In particular, near the bed the production of turbulence exceeded the rate of dissipation and the mean velocity profile conformed reasonably well with a logarithmic variation. The Reynolds stresses also decreased approximately linearly with elevation from the bed. Further from the bed, a region where the production and rate of dissipation were of similar magnitude was also found, consistent with equilibrium conditions. While instances of exceptions to these forms were observed, in general the results reinforce that the site was suitable for testing universal models which describe the turbulent structure in the water column.

The observations have provided further support for the applicability of steady, two-dimensional open-channel flow results to describe the turbulence anisotropy, and scales in fast-flowing, well-mixed tidal channels with weak wave action. In particular, there is a close relationship between the instantaneous Reynolds stress and turbulent kinetic energy, which therefore provides support for the use of simple turbulence closure models. While no flow visualization was available, the higher-order velocity statistics demonstrate that the Reynolds stress at $z/h = 0.1$ is highly intermittent. The good agreement of the quadrant analyses with laboratory results also suggests that the intermittency in the boundary layer in simple rapid flows such as at Islay are likely to be due to a well-defined process of sweeping and ejection of horseshoe-like vortices in the boundary layer.

Data accessibility. Data are available in the electronic supplementary material.

Authors' contributions. I.A.M. carried out the data analysis and prepared the manuscript under the guidance of R.N.S. and R.G.J.F.

Competing interests. We declare we have no competing interests.

Funding. The support of the Bright Futures Top Achiever Doctoral Scholarship is acknowledged.

Acknowledgements. The authors gratefully acknowledge the support of Andritz-Strom Hammerfest, ScottishPower Renewables and Partrac Ltd for provision of the dataset.

References

1. Milne IA. 2014 An experimental investigation of turbulence and unsteady loading on tidal turbines. PhD thesis. Department of Mechanical Engineering, The University of Auckland, New Zealand.
2. Milne IA, Day AH, Sharma RN, Flay RGJ. 2016 The characterisation of the hydrodynamic loads on tidal turbines due to turbulence. *Renew. Sustain. Energy Rev.* **56**, 851–864. (doi:10.1016/j.rser.2015.11.095)
3. Stacey MT, Monismith SG, Burau JR. 1999 Measurements of Reynolds stress profiles in unstratified tidal flow. *J. Geophys. Res.* **104**, 10 933–10 949. (doi:10.1029/1998JC900095)
4. Nezu I, Nakagawa H. 1993 *Turbulence in open-channel flows*. Rotterdam, The Netherlands: AA Balkema.
5. Grant HL, Stewart RW, Moilliet A. 1962 Turbulence spectra from a tidal channel. *J. Fluid Mech.* **12**, 241–268. (doi:10.1017/S002211206200018X)

6. Bowden KF, Howe MR. 1963 Observations of turbulence in a tidal current. *J. Fluid Mech.* **17**, 271–284. (doi:10.1017/S0022112063001300)
7. Heathershaw AD. 1979 The turbulent structure of the bottom boundary layer in a tidal current. *Geophys. J. Int.* **58**, 395–430. (doi:10.1111/j.1365-246X.1979.tb01032.x)
8. Soulsby RL. 1977 Similarity scaling of turbulence spectra in marine and atmospheric boundary layers. *J. Phys. Oceanogr.* **7**, 9340–937. (doi:10.1175/1520-0485(1977)007<0934:SSOTSI>2.0.CO;2)
9. Gross TF, Nowell ARM. 1985 Spectral scaling in a tidal boundary layer. *J. Phys. Oceanogr.* **15**, 496–508. (doi:10.1175/1520-0485(1985)015<3C0496:SSIATB>3E2.0.CO;2)
10. Kolmogorov AN. 1941 The local structure of turbulence in incompressible viscous fluid for very large Reynolds numbers. *Dokl. Akad. Nauk SSSR* **30**, 376–387.
11. Lien R-C, Sanford TB. 2000 Spectral characteristics of velocity and vorticity fluxes in an unstratified turbulent boundary layer. *J. Geophys. Res. Oceans* **105**, 8659–8672. (doi:10.1029/2000JC900031)
12. Walter RK, Nidzieko NJ, Monismith SG. 2011 Similarity scaling of turbulence spectra and cospectra in a shallow tidal flow. *J. Geophys. Res.* **116**, C10019. (doi:10.1029/2011JC007144)
13. Osalusi E, Side J, Harris R. 2009 Reynolds stress and turbulence estimates in bottom boundary layer of Fall of Warness. *Int. J. Heat Mass Transf.* **36**, 412–421. (doi:10.1016/j.icheatmasstransfer.2009.02.004)
14. Sellar B, Harding S, Richmond M. 2015 High-resolution velocimetry in energetic tidal currents using a convergent-beam acoustic Doppler profiler. *Meas. Sci. Technol.* **26**, 085801. (doi:10.1088/0957-0233/26/8/085801)
15. Thomson J, Polagye B, Durgesh V, Richmond MC. 2012 Measurements of turbulence at two tidal energy sites in Puget Sound, WA. *IEEE J. Oceanic Eng.* **37**, 363–374. (doi:10.1109/JOE.2012.2191656)
16. McCaffrey K, Fox-Kemper B, Hamlington PE, Thomson J. 2015 Characterization of turbulence anisotropy, coherence, and intermittency at a prospective tidal energy site: observational data analysis. *Renew. Energy* **76**, 441–453. (doi:10.1016/j.renene.2014.11.063)
17. Milne IA, Sharma RN, Flay RGJ, Bickerton S. 2013 Characteristics of the turbulence in the flow at a tidal stream power site. *Phil. Trans. R. Soc. A* **371**, 20120196. (doi:10.1098/rsta.2012.0196)
18. Lohrmann A, Hackett B, Red LP. 1990 High resolution measurements of turbulence, velocity and stress using a pulse-to-pulse coherent sonar. *J. Geophys. Res. Oceans* **105**, 8659–8672. (doi:10.1175/1520-0426(1990)007<0019:HRMOTV>2.0.CO;2)
19. Wiles PJ, Rippeth TP, Simpson JH, Hendricks PJ. 2006 A novel technique for measuring the rate of dissipation in the marine environment. *Geophys. Res. Lett.* **33**, L21608. (doi:10.1029/2006GL027050)
20. Lu SS, Willmarth WW. 1973 Measurements of the structure of the Reynolds stress in a turbulent boundary layer. *J. Fluid Mech.* **60**, 481–511. (doi:10.1017/S0022112073000315)
21. Lueck RG, Lu Y. 1997 The logarithmic layer in a tidal channel. *Cont. Shelf Res.* **17**, 1785–1801. (doi:10.1016/S0278-4343(97)00049-6)
22. Busch NE. 1973 On the mechanics of atmospheric turbulence. In *Workshop on micrometeorology* (ed. DA Haugen), pp. 1–65. Boston, MA: American Meteorological Society.
23. Bradshaw P, Ferriss DH, Atwell NP. 1967 Calculation of boundary-layer development using the turbulent energy equation. *J. Fluid Mech.* **28**, 593–616. (doi:10.1017/S0022112067002319)
24. Gross TF, Nowell ARM. 1983 Mean flow and turbulence scaling in a tidal boundary layer. *Cont. Shelf Res.* **2**, 109–126. (doi:10.1016/0278-4343(83)90011-0)
25. Townsend AA. 1976 *The structure of turbulent shear flow*. New York, NY: Cambridge University Press.
26. Bowden KF, Ferguson SR. 1980 Variation with height of the turbulence in a tidally-induced bottom boundary layer. In *Marine turbulence, Proc. of the 11th Int. Leige Colloquium on Ocean Hydrodynamics* (ed. J. Nihoul), pp. 258–286. New York, NY: Elsevier Science.
27. Diedrich FW, Drischler JA. 1957 Effect of spanwise variations in gust intensity on the lift due to atmospheric turbulence. NACA Technical Note 3920, National Advisory Committee for Aeronautics, Langley Field, VA, USA.
28. Kaimal JC, Wyngaard JC, Izumi Y, Cote OR. 1972 Spectral characteristics of surface-layer turbulence. *Q. J. R. Meteorol. Soc.* **98**, 563–589. (doi:10.1002/qj.49709841707)
29. Antonia RA, Luxton RE. 1971 The response of a turbulent boundary layer to a step change in surface roughness. Part 1: smooth to rough. *J. Fluid Mech.* **48**, 721–761. (doi:10.1017/S0022112071001824)